Field-induced dissociation of two-dimensional excitons in transition metal dichalcogenides

Kamban, Høgni Carlsson; Pedersen, Thomas Garm

Published in:
Physical Review B

DOI (link to publication from Publisher):
10.1103/PhysRevB.100.045307

Publication date:
2019

Document Version
Publisher's PDF, also known as Version of record

Field-induced dissociation of two-dimensional excitons in transition metal dichalcogenides

Høgni C. Kamban* and Thomas G. Pedersen
Department of Materials and Production, Aalborg University, DK-9220 Aalborg Øst, Denmark
and Center for Nanostructured Graphene (CNG), DK-9220 Aalborg Øst, Denmark

(Received 8 May 2019; published 17 July 2019)

Generation of photocurrents in semiconducting materials requires dissociation of excitons into free charge carriers. While thermal agitation is sufficient to induce dissociation in most bulk materials, an additional push is required to induce efficient dissociation of the strongly bound excitons in monolayer transition metal dichalcogenides (TMDs). Recently, static in-plane electric fields have proven to be a promising candidate. In the present paper, we introduce a numerical procedure, based on exterior complex scaling, capable of computing field-induced exciton dissociation rates for a wider range of field strengths than previously reported in the literature. We present both Stark shifts and dissociation rates for excitons in various TMDs calculated within the Mott-Wannier model. Here, we find that the field-induced dissociation rate is strongly dependent on the dielectric screening environment. Furthermore, applying weak-field asymptotic theory to the Keldysh potential, we are able to derive an analytical expression for exciton dissociation rates in the weak-field region.

DOI: 10.1103/PhysRevB.100.045307

I. INTRODUCTION

Interest in two-dimensional transition-metal dichalcogenide (TMD) semiconductors has increased substantially in recent years due to their exceptional electronic and optical properties. They have a wide range of applications, including photodetectors [1–3], light-emitting diodes [4], solar cells [5,6], and energy storage devices [7–9], to name a few. One of the most important implications of the reduced screening in two-dimensional TMDs is the comparatively large exciton binding energy [10–13]. Such excitons may significantly reduce the efficiency of solar cells and photodetectors, as these devices require the dissociation of excitons into free charge carriers to generate an electrical current. Excitons in bulk semiconductors will usually dissociate by thermal agitation alone due to their low binding energies. This is not the case for their two-dimensional counterparts, however, and it is therefore of great interest to obtain efficient methods of inducing exciton dissociation in TMD monolayers. Dissociation induced by in-plane static electric fields has gained attention lately. For instance, dissociation rates for two-dimensional excitons in MoS_2 were theoretically investigated in Refs. [14] and [15], and for various bulk TMDs in [13].

Recently, the first systematic experimental study of field-induced dissociation of two-dimensional excitons in monolayer WSe_2 encapsulated by hBN was carried out [16]. It was found that the limiting factor in generating photocurrents when a weak in-plane field was present was the dissociation rate of electron-hole pairs. That work also showed that the photocurrent generated in fields weaker than 15 V/μm was accurately predicted by the Mott-Wannier model [17,18]. Nevertheless, these weak-field dissociation rates proved troublesome to obtain numerically [16], and they were therefore extrapolated by fitting to the rate of a two-dimensional hydrogen atom [19]. In the present paper, we introduce a numerical method capable of computing exciton dissociation rates for significantly weaker fields with no compromise on the accuracy for stronger fields. It is based on the complex scaling approach [20,21] that was used in Refs. [14] and [16], but, rather than rotating the entire spatial region into the complex plane, we rotate the radial coordinate only in an exterior region $r > R$. For sufficiently weak fields, we show that the rates can be obtained analytically based on the recently developed weak-field asymptotic theory (WFAT) [22], which greatly simplifies their calculation. Furthermore, we show that the weak-field ionization rate of two-dimensional hydrogen is a special case of a more general formula for dissociation of a two-dimensional two-particle system.

II. TMD EXCITON IN ELECTROSTATIC FIELD

Throughout the present paper, excitons will be modeled as electron-hole pairs described by the two-dimensional Wannier equation [17,18], which reads (atomic units are used throughout)

$$\left[-\frac{1}{2\mu}\nabla^2 - w(\kappa \boldsymbol{r})\right]\psi(\boldsymbol{r}) = E\psi(\boldsymbol{r}), \tag{1}$$

where μ is the reduced exciton mass, $\boldsymbol{r} = \boldsymbol{r}_e - \boldsymbol{r}_h$ is the relative in-plane coordinate of the electron-hole pair, $\kappa = (\kappa_a + \kappa_b)/2$ is the average dielectric constant of the materials above and beneath the TMD sheet, and w is a screened Coulomb attraction. It is well known that screening in two-dimensional semiconductors, such as TMDs, is inherently nonlocal [23,24], i.e., momentum-dependent, and can be approximated by the linearized form $\epsilon(\boldsymbol{q}) = \kappa + r_0 q$, where $\boldsymbol{q}$ is the wave vector, and the so-called screening length r_0 can be related to the polarizability of the sheet [23]. The interaction w may then be obtained as the inverse Fourier transform of $2\pi[\epsilon(\boldsymbol{q})q]^{-1}$, where $2\pi/q$ is the 2D Fourier transform of $1/r$.

*Corresponding author: hck@mp.aau.dk

The resulting interaction is given by the Keldysh [24,25] form

$$w(\boldsymbol{r}) = \frac{\pi}{2r_0}\left[H_0\left(\frac{r}{r_0}\right) - Y_0\left(\frac{r}{r_0}\right)\right], \tag{2}$$

where H_0 is the zeroth-order Struve function and Y_0 is the zeroth-order Bessel function of the second kind [26].

When an in-plane electrostatic field is applied to the exciton, Eq. (1) is modified to include a perturbation term

$$\left[-\frac{1}{2\mu}\nabla^2 - w(\kappa\boldsymbol{r}) + \boldsymbol{\varepsilon}\cdot\boldsymbol{r}\right]\psi(\boldsymbol{r}) = E\psi(\boldsymbol{r}). \tag{3}$$

In the present paper, we will restrict ourselves to electric fields pointing along the x-axis, i.e., $\boldsymbol{\varepsilon} = \varepsilon\boldsymbol{e}_x$. As is evident, the form of Eq. (3) is the same as that of the two-dimensional hydrogen atom in a static electric field [19], albeit with a different potential. It should therefore come as no surprise that excitons perturbed by an electrostatic field will eventually dissociate. An important distinction, however, is that the excitons will recombine if they are not dissociated [16,27]. This field-free recombination rate is in competition with the field-induced dissociation. For practical applications, recombination [28–30] and other forms of exciton decay (such as defect-assisted recombination [31] and exciton-exciton annihilation [32]), which do not yield free charge carriers, are often undesired.

The field-induced dissociation rate Γ is connected to the nonvanishing imaginary part of the energy eigenvalue in the presence of an electric field by the relation $\Gamma = -2\,\mathrm{Im}E$ [13,14,16,19]. The desired eigenvalues are therefore unobtainable through conventional Hermitian methods. Rather, one should solve Eq. (3) subject to regularity and outgoing boundary conditions [22,33]. This is a nontrivial task in all but the simplest cases, and in practice one usually computes the resonance energies by complex scaling of the Hamiltonian [20,21].

III. EXCITON DISSOCIATION

In its simplest form, complex scaling corresponds to rotating the radial coordinate into the complex plane uniformly [20,21], $r \to \exp(i\phi)r$, where ϕ is a fixed real-valued angle (note that if ϕ is chosen complex, the coordinate will simply be stretched as well as rotated). This transformation, referred to as uniform complex scaling (UCS), turns the outgoing waves mentioned above into exponentially decaying waves, provided that ϕ is chosen large enough [34]. Thus, the complex scaled resonance wave functions are square integrable, and the resonance energies can be obtained by solving Eq. (3) with the scaled operator and the boundary condition $\psi(r \to \infty) = 0$. This approach has been used to obtain the dissociation rates of two-dimensional TMD excitons in Refs. [14,16]. Nevertheless, as was discussed briefly in Ref. [16], numerical difficulties arise when the electric field becomes sufficiently weak. This is because the important region for weak fields is sufficiently far from the origin that the uniformly complex scaled resonance wave function has (numerically) vanished prior to reaching this region. By utilizing the so-called exterior complex scaling (ECS) approach

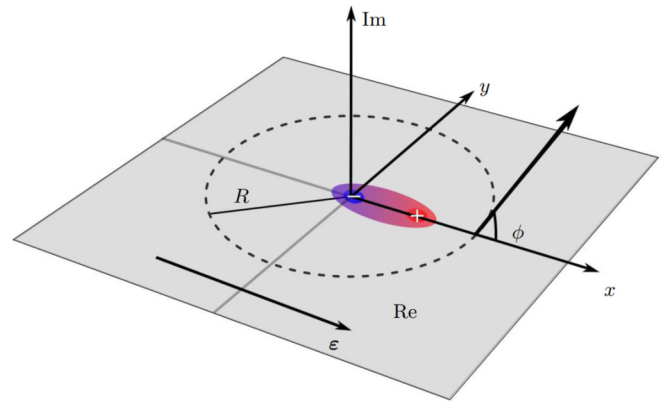

FIG. 1. Sketch of the two-dimensional exciton in the xy-plane with the radial coordinate rotated into the complex plane by an angle of ϕ for $r > R$.

[34–37], combined with a finite-element (FE) representation of the wave function, we are able to compute dissociation rates for significantly weaker fields, as we now demonstrate.

As the name suggests, ECS transforms the radial coordinate outside a scaling radius R,

$$r \to \begin{cases} r & \text{for } r < R, \\ R + (r-R)e^{i\phi} & \text{for } r > R, \end{cases} \tag{4}$$

where ϕ is the angle of rotation, as illustrated in Fig. 1. The partitioning of the radial coordinate is efficiently dealt with by an FE basis representation, the details of which can be found in Appendix A. Fig. 2 shows the Stark shift and dissociation rate of the ground-state exciton as functions of in-plane field strength for four important materials in various dielectric environments. The screening lengths and reduced masses used in the calculations are obtained from Ref. [38]. As is evident, the dissociation rate increases rapidly with increasing field strength. The rates can also be seen to be strongly dependent on the screening environment, which is to be expected as increased screening leads to reduced binding energies. It is therefore possible to tune the dissociation rates of the TMDs as desired within a certain range. For example, encapsulating the TMDs in hBN (with $\kappa = 4.9$ [11]) increases the dissociation rates by several orders of magnitude compared to their free-space counterparts. Rates for MoS_2, MoS_2/hBN, and hBN/MoS_2/hBN were presented in Ref. [14] for fields stronger than 50 V/μm. However, the experimental study of hBN/WSe_2/hBN in Ref. [16] suggests that exciton dissociation rates are the limiting factor in generation of photocurrents for applied fields weaker than 15 V/μm in this material. For stronger fields, the photocurrent measurements deviate from the field-induced rates predicted by the Wannier model, and other limitations dominate [16]. We expect to see the same effect for the other TMDs, and we furthermore expect this threshold field to increase as the screening is reduced.

In weak fields, the Stark shifts in Fig. 2 can be seen to vary approximately as ε^2, in agreement with the lowest-order perturbation theory expansion of the energy $E \approx E_0 - \frac{1}{2}\alpha\varepsilon^2$, where E_0 is the unperturbed ground-state energy and α is the exciton polarizability. The shape of the shift is in agreement

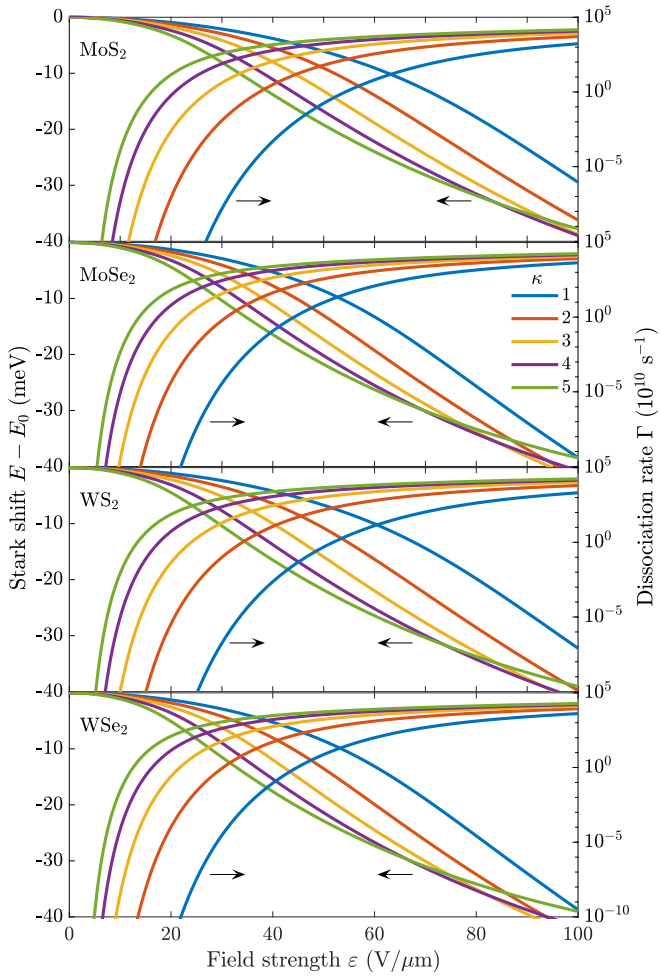

FIG. 2. Exciton Stark shift and dissociation rate of the ground-state exciton for four important materials in various dielectric environments.

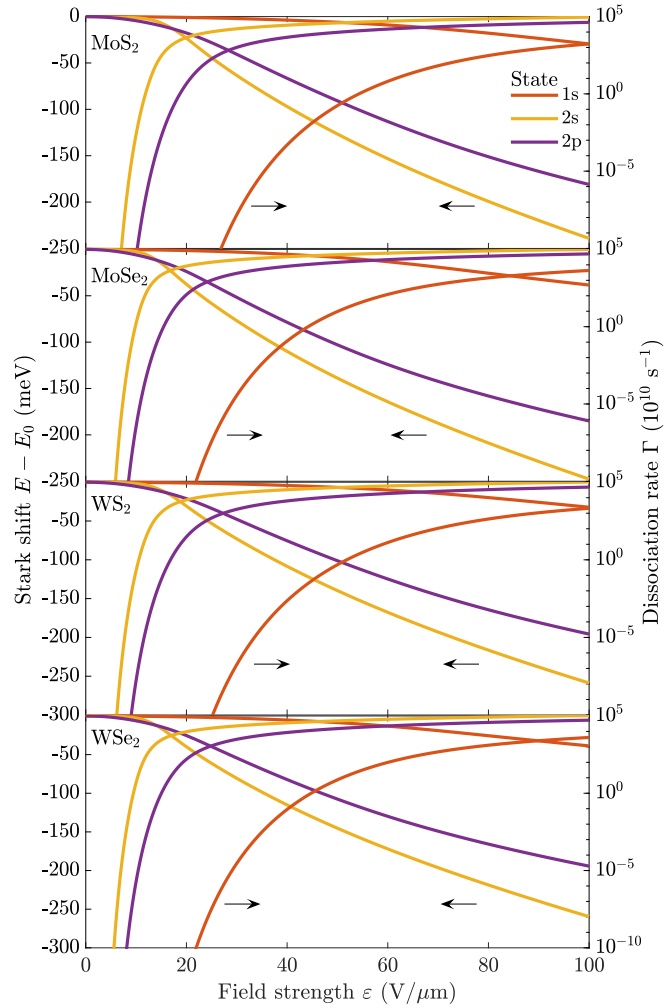

FIG. 3. Stark shift and dissociation rates for excitons occupying either the $1s$, $2s$, or $2p$ state in TMDs located in free space ($\kappa = 1$).

with those observed for similar systems; the energy initially decreases rapidly with field strength and then levels off as the field strength increases [19]. A more detailed analysis of the shift in the weak-field region will be made in Sec. V.

The resonance discussed above corresponds to dissociation of an exciton in its ground state. Meanwhile, excitation by high-energy photons may produce higher excitons. It is therefore interesting to analyze the dissociation rates of excited states. The numerical procedure outlined in Appendix A is perfectly capable of handling excited states, and in Fig. 3 we show Stark shifts and dissociation rates for excitons occupying either the $1s$, $2s$, or $2p$ state in four different TMDs located in free space ($\kappa = 1$). As expected, the dissociation rates for the excited states are much larger than those of the ground state, and for weak electric fields in particular. This, along with the fast decay of excited states to the ground state, means that the limiting factor in generation of photocurrents in weak in-plane electric fields is dominated by the dissociation rate of ground-state excitons. This explains the excellent agreement between photocurrent measurements and calculated ground-state dissociation in Ref. [16] for weak electric fields. We also observe a substantially larger Stark shift in the $2s$ and $2p$ states, in agreement with expectations.

IV. WEAK-FIELD ASYMPTOTIC THEORY

Even with the improved numerical procedure, the dissociation rates for extremely weak fields are unobtainable. In fact, any numerical procedure with finite-precision arithmetic fails for sufficiently weak fields, when the ratio $\Gamma/|E_0|$ approaches the round-off error [39,40]. Fortunately, with the recent development of weak-field asymptotic theory (WFAT) [22], we are able to take advantage of the simple asymptotic form of the Keldysh potential and calculate the weak-field dissociation rates analytically. To this end, we first simplify Eq. (3) by introducing the scaling relations

$$\tilde{r}_0 = \frac{\mu}{\kappa^2} r_0, \quad \tilde{\boldsymbol{r}} = \frac{\mu}{\kappa} \boldsymbol{r}, \quad \text{and} \quad \tilde{\boldsymbol{\varepsilon}} = \frac{\kappa^3}{\mu^2} \boldsymbol{\varepsilon}, \tag{5}$$

which lead to

$$E(\mu, \kappa, r_0, \varepsilon) = \frac{\mu}{\kappa^2} E(1, 1, \tilde{r}_0, \tilde{\varepsilon}). \tag{6}$$

Thus, the only nontrivial parameters are $\tilde{r}_0$ and $\tilde{\varepsilon}$, and the analysis in the following will therefore be restricted to the simplified problem

$$\left[-\tfrac{1}{2}\nabla^2 - w(\boldsymbol{r}) + \boldsymbol{\varepsilon} \cdot \boldsymbol{r}\right]\psi(\boldsymbol{r}) = E\psi(\boldsymbol{r}), \tag{7}$$

from which Stark shifts and dissociation rates can be obtained using Eq. (6). Note that in order to simplify the notation, the tilde has been omitted in Eq. (7) as well as in the following. Therefore, unless explicitly stated otherwise, r, r_0, ε, and E in the following refer to the scaled parameters. As discussed in the previous section, the limiting factor in generating photocurrents is the dissociation rate of the ground-state exciton. For this reason, we restrict our analysis in the following to the ground state.

The potential in Eq. (7) has the large-r behavior [26]

$$w(\boldsymbol{r}) = \frac{1}{r} + O\left(\frac{r_0^2}{r^3}\right), \tag{8}$$

which has the form required to use WFAT. A leading-order expression for the weak-field dissociation rate was derived for a three-dimensional system in Ref. [22] and extended to first order in ε in Ref. [39]. We shall only consider the leading-order approximation here. By modifying the approach in Ref. [22] to two dimensions, we find that the weak-field dissociation rate for the ground state of Eq. (7) is given by

$$\Gamma \approx |g_0|^2 W_0(\varepsilon), \tag{9}$$

with the asymptotic coefficient and field factor [41,42] given by

$$g_0 = \lim_{v\to\infty} v^{1/2-1/k} e^{kv/2} \int_0^\infty \varphi_0(u)\psi_0\left(\frac{u+v}{2}\right)\frac{1}{\sqrt{u}}du \tag{10}$$

and

$$W_0(\varepsilon) = k\left(\frac{4k^2}{\varepsilon}\right)^{2/k-1/2} \exp\left(-\frac{2k^3}{3\varepsilon}\right), \tag{11}$$

respectively. Here, $k = \sqrt{-2E_0}$, and u and v are the parabolic cylindrical coordinates defined by

$$u = r + x, \quad u \in [0, \infty), \tag{12}$$

$$v = r - x, \quad v \in [0, \infty). \tag{13}$$

The functions appearing in Eq. (10) are the unperturbed ground state ψ_0 and

$$\varphi_n(u) = \left[\frac{\sqrt{k}n!}{(n-1/2)!}\right]^{1/2} L_n^{(-1/2)}(ku)e^{-ku/2}, \tag{14}$$

with $L_n^{(\alpha)}(x)$ a generalized Laguerre polynomial [26]. To obtain the weak-field dissociation rate from Eq. (9), one therefore needs the unperturbed binding energy E_0 and the asymptotic coefficient g_0 of the simplified problem. Once they have been obtained, the physical weak-field dissociation rate for arbitrary monolayer TMDs can be obtained by scaling back to the original units, cf. Eq. (6),

$$\Gamma(\mu, \kappa, r_0, \varepsilon) = \frac{\mu}{\kappa^2}\Gamma(1, 1, \tilde{r}_0, \tilde{\varepsilon}). \tag{15}$$

We now turn to computing the asymptotic coefficient g_0.

Computing the asymptotic coefficient

Finding g_0 given by Eq. (10) requires an accurate representation of the wave function for large v. Note that a traditional basis expansion (e.g., a Gaussian basis) is generally not accurate enough, as only the most slowly decaying functions will contribute in this region. This problem was partially circumvented in Ref. [42] by using a Gaussian basis with optimized exponents. Here, we will implement Numerov's finite-difference scheme, which can accurately and efficiently construct the unperturbed wave function in the asymptotic region. The technical details can be found in Appendix B. As a preliminary, it is convenient to relate g_0 to the radial wave function. The ground state of a potential with cylindrical symmetry satisfies

$$\psi_0(r) \sim C_0 r^{1/k-1/2} e^{-kr} \quad \text{for } r \to \infty, \tag{16}$$

where C_0 is a constant. Using Eq. (16) in Eq. (10) leads to the relation

$$g_0 = \frac{2^{1/2-1/k}\pi^{1/4}C_0}{k^{1/4}}. \tag{17}$$

The problem of finding g_0 has therefore been reduced to obtaining the asymptotic coefficient of the radial wave function. It can be found by taking the limit

$$C_0 = \lim_{r\to\infty} \psi_0 r^{1/2-1/k} e^{kr}. \tag{18}$$

Note that in the unscreened limit ($r_0 \to 0$), $k = 2$ and $\psi_0 = 2^{3/2}\pi^{-1/2}\exp[-(u+v)]$ [43], which leads to $g_0 = 2^{5/4}\pi^{-1/4}$, and Eq. (9) is therefore in agreement with the expression found in Ref. [19] for the two-dimensional hydrogen atom. In practice, we find C_0 by fitting Eq. (18) to the asymptotic expansion

$$D(r) = \sum_{n=0}^{4} \frac{d_n}{r^n}, \tag{19}$$

in a stable region (see Appendix B), as described in Ref. [42]. The asymptotic coefficient C_0 is then obtained by taking the limit $\lim_{r\to\infty} D = d_0$. The computational method above takes advantage of the fact that a high-order finite-difference scheme is able to accurately reproduce the wave function for large r. Recently, however, integral representations for the asymptotic coefficient that are insensitive to the wave function tail have been derived for a three-dimensional system [44,45]. This suggests that one may get away with using a sufficiently accurate representation of the wave function only in an interior region. We shall use the integral equations as a check to ensure the accuracy of the scheme presented above. To derive the corresponding equation for our two-dimensional system, we introduce the reference function Ω as a solution to

$$\left[-\frac{1}{2}\nabla^2 - \frac{1}{r} + \frac{k^2}{2}\right]\Omega_n(r) = 0. \tag{20}$$

The relevant function for the asymptotic coefficient of the ground state is

$$\Omega_0(r) = -2^{\frac{1}{k}+\frac{1}{2}} k^{\frac{1}{k}-\frac{1}{2}} \Gamma\left(\frac{1}{2} - \frac{1}{k}\right) e^{-kr} M\left(\frac{1}{2} - \frac{1}{k}; 1; 2kr\right), \tag{21}$$

where M is a confluent hypergeometric function [26]. If the exciton energy coincides with one of the energies of the

TABLE I. Binding energy $E_0(1, 1, \tilde{r}_0)$ and asymptotic coefficient g_0 of the simplified problem for four important materials in different dielectric environments.

	MoS_2		$MoSe_2$		WS_2		WSe_2	
κ	E_0	g_0	E_0	g_0	E_0	g_0	E_0	g_0
1	0.0714	0.00098	0.0659	0.00057	0.0921	0.0044	0.0801	0.0020
2	0.1907	0.0889	0.1773	0.0707	0.2392	0.1671	0.2113	0.1200
3	0.3200	0.3210	0.2995	0.2805	0.3928	0.4650	0.3512	0.3829
4	0.4474	0.5695	0.4210	0.5195	0.5392	0.7323	0.4870	0.6420
5	0.5680	0.7796	0.5370	0.729	0.6740	0.9380	0.6142	0.8515

two-dimensional hydrogen atom

$$E_n^{(\mathrm{hydr})} = \frac{1}{2(n-1/2)^2}, \tag{22}$$

where $n = 1, 2, \ldots$ [43], the confluent hypergeometric function in Eq. (21) reduces to a polynomial of finite degree, and Ω_0 will vanish as r tends to infinity. In practical calculations, this is hardly ever the case and the reference function will therefore be exponentially increasing (see Ref. [46] for a discussion of the case in which $E_0 \approx E_n^{(\mathrm{hydr})}$),

$$\Omega(r) \sim -k^{-1} r^{-1/2-1/k} e^{kr} \quad \text{for} \quad r \to \infty. \tag{23}$$

Integrating by parts and using Eqs. (16) and (23) when r tends to infinity, we find

$$C_0 = \int_0^\infty \Omega_0(r)\left[\frac{1}{2}\nabla^2 + \frac{1}{r} - \frac{k^2}{2}\right]\psi_0(r) r\, dr, \tag{24}$$

which, using Eq. (7) with $\varepsilon = 0$, can be reduced to

$$C_0 = \int_0^\infty \Omega_0(r)\left[\frac{1}{r} - w(r)\right]\psi_0(r) r\, dr. \tag{25}$$

The integrand in Eq. (25) is a product of an exponentially increasing function Ω_0 and an exponentially decreasing function ψ_0. Such an integral need not be convergent. Nevertheless, as is evident from the large-r behavior of these functions [see Eqs. (16) and (23)], the exponential terms cancel for r tending to infinity, resulting in the integrand tending to zero sufficiently quickly for the integral to converge. We have checked that Eqs. (18) and (25) agree when using the numerically exact wave function. The asymptotic coefficients and binding energies of the simplified Wannier problem for four important materials are presented in Table I. Note that these binding energies increase with κ. This is because the binding energies of the simplified problem increase when $\tilde{r}_0$ decreases and $\tilde{r}_0$ is proportional to κ^{-2}. In Fig. 4, we compare the dissociation rates for excitons in MoS_2 and WSe_2 given by the weak-field formula Eq. (9) to the numerically exact dissociation rates. As can be seen, the agreement between the weak field and the fully numerical results is reasonable for fields lower than 50 V/μm and improves as the field strength decreases. For $\varepsilon \lesssim \kappa^{-1/2}$ 20 V/μm the agreement in Fig. 4 becomes excellent.

V. STARK SHIFT

Applying perturbation theory to the ground state of a system with cylindrical symmetry leads to the well-known result

$$E = E_0 - \tfrac{1}{2}\alpha\varepsilon^2 + O(\varepsilon^4), \tag{26}$$

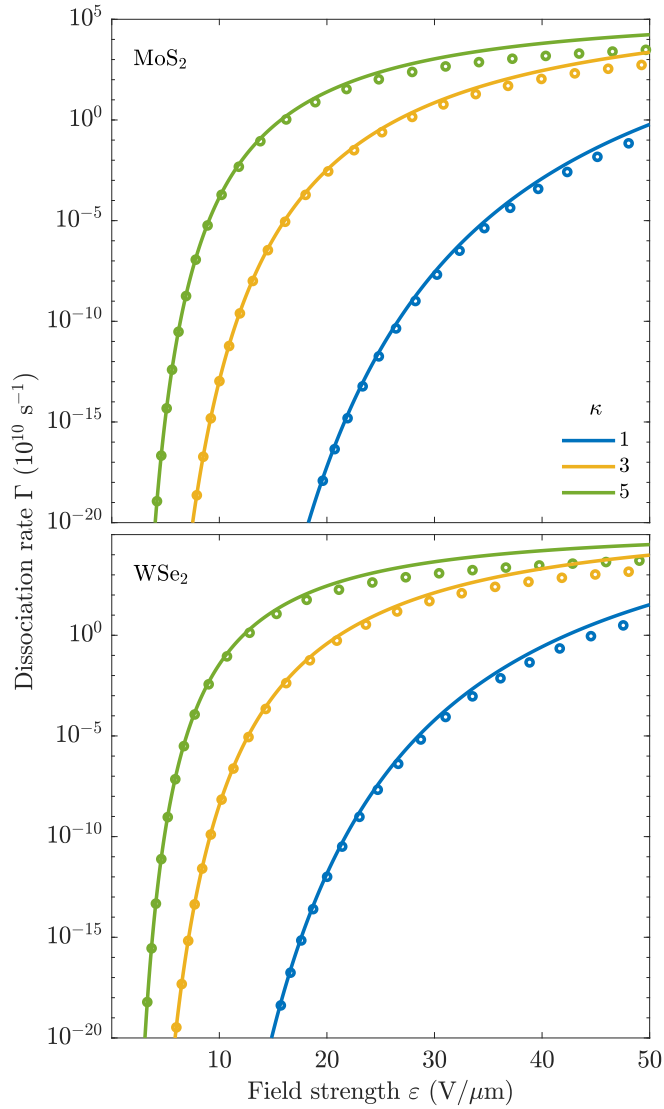

FIG. 4. Exciton dissociation rates for MoS_2 (upper) and WSe_2 (lower) encapsulated by various dielectric media. The circles are the numerically exact results obtained by the method in Appendix A (same as those in Fig. 2). The solid lines correspond to the weak-field formula Eq. (9) with the parameters found in Table I.

TABLE II. Exciton polarizability α for various TMDs in different dielectric environments in units of 10^{-18} eV(m/V)^2 calculated from Eq. (27) with ψ_0 and ψ_1 expanded in an FE basis with a spacing of 1 a.u.

κ	MoS_2 α	$MoSe_2$ α	WS_2 α	WSe_2 α
1	4.59	6.24	5.04	6.24
2	6.31	8.46	7.30	8.78
3	8.48	11.22	10.25	12.02
4	11.18	14.63	14.09	16.14
5	14.54	18.81	19.00	21.32

where α is the static polarizability. A shortcoming of perturbation theory is that it predicts the energy as a function of field strength to be purely real, which, as seen in the previous sections, is obviously not correct for a system in which dissociation is possible. Nevertheless, the nonperturbative behavior of the resonance energy can be reproduced by utilizing the first few perturbation coefficients together with the hypergeometric resummation technique [47]. This approach was used in Ref. [19] with great success for low-dimensional hydrogen. In the present section, we wish to analyze to what extent the change in the real part of the resonance energy, i.e., the exciton Stark shift, can be predicted by standard second-order perturbation theory (for previous work on exciton Stark shifts in TMDs, see Refs. [14,15,48,49]). To this end, we calculate the exciton polarizability given by

$$\alpha = -2\langle\psi_0|r\cos\theta|\psi_1\rangle, \tag{27}$$

where the first-order correction ψ_1 is a solution to the Dalgarno-Lewis [50] equation

$$\left[-\frac{1}{2\mu}\nabla^2 - w(\kappa\boldsymbol{r}) - E_0\right]\psi_1 = -r\cos\theta\psi_0, \tag{28}$$

and will therefore be of the form $\psi_1 = \cos\theta f(r)$, where f is a purely radial function. Expanding ψ_0 and ψ_1 in a finite-element basis (without complex scaling), as described in Appendix A, Eq. (28) can be solved and the polarizability found (for alternative methods of finding the polarizability, see Ref. [48]). The exciton polarizability for various TMDs in different environments can be found in Table II, and Fig. 5 shows a comparison between the shift in the real part of the complex resonance energy and the perturbation series in Eq. (26). Evidently, a good agreement is found in the weak-field region. Furthermore, excitons in environments with large dielectric screening begin to deviate from their second-order expansion for weaker fields than their free-space counterparts. This is to be expected, as the binding energies of excitons with heavily screened interactions are lower and the characteristic fields of these excitons are therefore weaker.

VI. SUMMARY

In the present work, electric-field-induced dissociation of TMD excitons has been investigated using both numerical and analytical approaches. The dissociation rates as functions of the in-plane field strength for excitons in monolayer MoS_2, $MoSe_2$, WS_2, and WSe_2 in various screening environments have been obtained. In particular, difficulties associated with dissociation rates in weak electric fields have been addressed and resolved. In this regard, an efficient numerical method capable of computing dissociation rates for a wide range of fields has been introduced. As the field becomes sufficiently weak, any numerical method with finite precision arithmetic breaks down, which calls for a different approach. We demonstrate that an analytical weak-field approximation is valid in this region, which makes the weak-field dissociation rates readily available for arbitrarily weak fields. Finally, the exciton Stark shift has been analyzed and compared to the results of second-order perturbation theory.

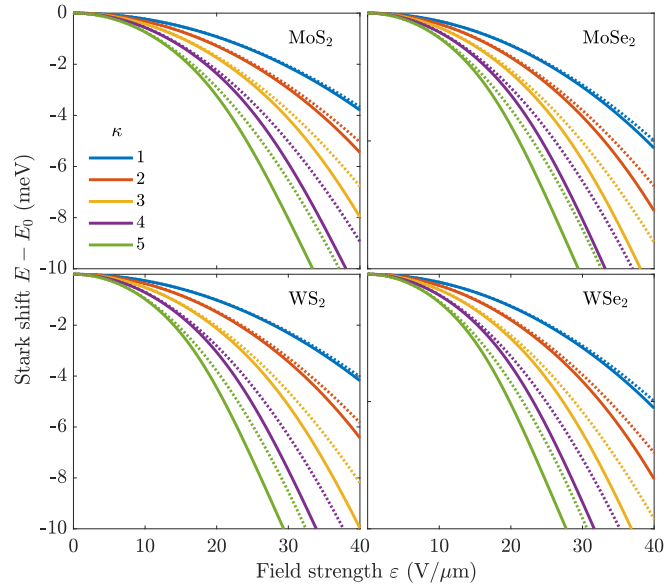

FIG. 5. Exciton Stark shift for four important TMDs in various dielectric environments. The solid lines correspond to the real part of the resonance energy, while the dotted lines show the shift predicted by perturbation theory, $E - E_0 \approx -\alpha\varepsilon^2/2$.

ACKNOWLEDGMENTS

The authors gratefully acknowledge financial support by the Center for Nanostructured Graphene (CNG), which is sponsored by the Danish National Research Foundation, Project No. DNRF103. Additionally, T.G.P. is supported by the QUSCOPE Center, sponsored by the Villum Foundation.

APPENDIX A: NUMERICAL PROCEDURE

To implement the finite-element (FE) approach, we first divide the radial grid into N segments $[r_{n-1}, r_n]$ for $n = 1, \ldots, N$. Following the procedure in Ref. [51], we introduce a set of p_n linearly independent functions $h_i^{(n)}$, where $i = 1, \ldots, p_n$ on each segment. These functions are then transformed into a different set of functions $f_i^{(n)}$, $i = 1, \ldots, p_n$, that vanish at the segment boundaries, except for the first and last function, which are required to equal unity at the lower and upper element boundaries, respectively. To

summarize,

$$f_i^{(n)}(r_{n-1}) = f_i^{(n)}(r_n) = 0, \tag{A1}$$

$$\text{except} \quad f_1^{(n)}(r_{n-1}) = f_{p_n}^{(n)}(r_n) = 1. \tag{A2}$$

We use Legendre polynomials $h_i^{(n)}(r) = P_{i-1}[y_n(r)]$, where y_n maps $[r_{n-1}, r_n]$ onto $[-1, 1]$, and $h_i^{(n)}$ is set equal to zero for $r \notin [r_{n-1}, r_n]$. Dirichlet boundary conditions are then implemented for some large $r_N \geqslant R$ by omitting the last function $f_{p_N}^{(N)}$. The scaling radius R is to be chosen to coincide with an element boundary. Note that if $r_N = R$, no complex scaling is implemented. The eigenstate can now be written as a sum of basis functions,

$$\psi(\boldsymbol{r}) = \sum_{m=0}^{M} \sum_{n=1}^{N} \sum_{i=1}^{p_n} c_i^{(m,n)} f_i^{(n)}(r) \cos(m\theta), \tag{A3}$$

where the radial part is resolved using the finite-element basis. Due to the cylindrical symmetry of the unperturbed problem, the angular dependence of the unperturbed eigenstates is the cylindrical harmonics $e^{im\theta}$. The angular part of the eigenstate is therefore resolved efficiently using a basis of cosine functions. To ensure continuity across the segment boundaries, we enforce

$$c_{p_{n-1}}^{(m,n-1)} = c_1^{(m,n)}, \quad n = 2, \ldots, N. \tag{A4}$$

To evaluate the radial part of the matrix elements, we use the Legendre quadrature rule [52].

We proceed by providing a recipe for constructing the overlap and Hamilton matrix, and we refer the interested reader to Refs. [34,51] and references therein for more details on the mathematical background. It is convenient to first construct segmentwise matrices containing only the radial part of the matrix elements. For segments with $r_n \leqslant R$ the procedure is familiar, and, as an example, the radial segmentwise overlap matrices are given by

$$S_{ij}^{(n)} = \int_0^\infty f_i^{(n)}(r) f_j^{(n)}(r) r\, dr \tag{A5}$$

$$\approx \sum_{k=1}^{K} f_i^{(n)}\left(r_k^{(n)}\right) f_j^{(n)}\left(r_k^{(n)}\right) r_k^{(n)} w_k^{(n)}, \tag{A6}$$

where $w_k^{(n)}$ and $r_k^{(n)}$ are the quadrature weights and sample points for the nth segment, respectively. For segments with $r_{n-1} \geqslant R$, the radial coordinate is transformed according to Eq. (4) and the matrix elements must be modified accordingly. The integral element dr must be multiplied by $e^{i\phi}$, and r must be replaced by the transformation in Eq. (4), all the while keeping the argument of the basis functions unchanged. As an example, the segmentwise overlap matrix becomes

$$S_{ij}^{(n)} \approx \sum_{k=1}^{K} \left\{ f_i^{(n)}\left(r_k^{(n)}\right) f_j^{(n)}\left(r_k^{(n)}\right) \left[R + \left(r_k^{(n)} - R\right) e^{i\phi}\right] w_k^{(n)} e^{i\phi} \right\}. \tag{A7}$$

The segmentwise matrices are then collected into the complete radial overlap matrix $\mathbf{S}_r$ such that the last row and column of each segmentwise matrix overlaps with the first row and column of the next (see Ref. [51] for a visual demonstration). This conveniently enforces Eq. (A4). The complete overlap matrix $\mathbf{S}$ is then a block-diagonal matrix with blocks consisting of $\pi(1 + \delta_{m0})\mathbf{S}_r$ for $m = 0, \ldots, M$. The Hamilton matrix can be constructed in a similar manner, keeping in mind that $\frac{d}{dr} f_i$ should be replaced by $e^{-i\phi} \frac{d}{dr} f_i$ for segments outside the scaling radius, and that the (untransformed) segmentwise kinetic matrix elements are given by

$$T_{ij}^{(n)} = \frac{1}{2} \int_{r_{n-1}}^{r_n} \frac{df_i}{dr} \frac{df_j}{dr} r\, dr, \tag{A8}$$

to comply with the correct definition of the kinetic energy in an FE basis [37,53]. The transformed Wannier equation is then readily solved as a matrix eigenvalue problem.

APPENDIX B: COMPUTATIONAL PROCEDURE FOR THE ASYMPTOTIC COEFFICIENT

Grid-based finite-difference methods (FDMs) are able to efficiently reproduce the correct behavior of the wave function for all values of r, as long as a dense enough grid is used. Numerov's method is a fourth-order FDM, on par with the fourth-order Runge-Kutta method. However, the advantage is that it is simpler to implement. The ground-state wave function can be presented in the form $\psi_0(r) = r^{-1/2} P(r)$, which transforms Eq. (7) (with $\varepsilon = 0$) to the differential equation

$$\frac{d^2 P(r)}{dr^2} + g(r) P(r) = 0, \tag{B1}$$

where

$$g(r) = \frac{1}{4r^2} + 2[E_0 + w(r)]. \tag{B2}$$

We now assume E_0 is known (it can easily be calculated by, e.g., diagonalizing a Gaussian basis or performing a variational calculation). Numerov's method then reduces this equation to the finite-difference equation

$$f_{n-1} P_{n-1} = (12 - 10 f_n) P_n - f_{n+1} P_{n+1}, \tag{B3}$$

where $P_n = P(r_n)$ and $f_n = 1 + (\Delta r)^2 g_n / 12$ with $g_n = g(r_n)$. The $N + 1$ discrete points r_n are defined as $r_n = n\Delta r$, where $n = 0, \ldots, N$ and $\Delta r = r_N / N$. The two initial points are then chosen as $P_N = 0$ for some large r_N and to comply with Eq. (16) for r_{N-1}. Integrating toward $r = 0$ then yields P at all r_n. The fitting procedure described in the main text is then implemented by fitting Eq. (18) to Eq. (19) in a region $r \in [(j-1)40, j40]$, where $j = 1, 2, \ldots$, until convergence to four significant digits. The same P is then used in Eq. (25) and the agreeing significant digits (up to fourth order) are presented in Table I.

[1] H. Wang, C. Zhang, W. Chan, S. Tiwari, and F. Rana, Nat. Commun. **6**, 8831 (2015).

[2] O. Lopez-Sanchez, D. Lembke, M. Kayci, A. Radenovic, and A. Kis, Nat. Nanotechnol. **8**, 497 (2013).

[3] Z. Yin, H. Li, H. Li, L. Jiang, Y. Shi, Y. Sun, G. Lu, Q. Zhang, X. Chen, and H. Zhang, ACS Nano **6**, 74 (2012).

[4] F. Withers, O. D. Pozo-Zamudio, A. Mishchenko, A. P. Rooney, A. Gholinia, K. Watanabe, T. Taniguchi, S. J. Haigh, A. K. Geim, A. I. Tartakovskii, and K. S. Novoselov, Nat. Mater. **14**, 301 (2015).

[5] O. Lopez-Sanchez, E. Alarcon Llado, V. Koman, A. Fontcuberta i Morral, A. Radenovic, and A. Kis, ACS Nano **8**, 3042 (2014).

[6] M. Bernardi, M. Palummo, and J. C. Grossman, Nano Lett. **13**, 3664 (2013).

[7] G. Du, Z. Guo, S. Wang, R. Zeng, Z. Chen, and H. Liu, Chem. Commun. **46**, 1106 (2010).

[8] M. Chhowalla, H. S. Shin, G. Eda, L.-J. Li, K. P. Loh, and H. Zhang, Nat. Chem. **5**, 263 (2013).

[9] J. M. Soon and K. P. Loh, Electrochem. Solid State Lett. **10**, A250 (2007).

[10] A. Ramasubramaniam, Phys. Rev. B **86**, 115409 (2012).

[11] S. Latini, T. Olsen, and K. S. Thygesen, Phys. Rev. B **92**, 245123 (2015).

[12] T. C. Berkelbach, M. S. Hybertsen, and D. R. Reichman, Phys. Rev. B **88**, 045318 (2013).

[13] T. G. Pedersen, S. Latini, K. S. Thygesen, H. Mera, and B. K. Nikolić, New J. Phys. **18**, 073043 (2016).

[14] S. Haastrup, S. Latini, K. Bolotin, and K. S. Thygesen, Phys. Rev. B **94**, 041401(R) (2016).

[15] B. Scharf, T. Frank, M. Gmitra, J. Fabian, I. Žutić, and V. Perebeinos, Phys. Rev. B **94**, 245434 (2016).

[16] M. Massicotte, F. Vialla, P. Schmidt, M. B. Lundeberg, S. Latini, S. Haastrup, M. Danovich, D. Davydovskaya, K. Watanabe, T. Taniguchi, V. I. Falko, K. Thygesen, T. G. Pedersen, and F. H. L. Koppens, Nat. Commun. **9**, 1633 (2018).

[17] G. H. Wannier, Phys. Rev. **52**, 191 (1937).

[18] F. L. Lederman and J. D. Dow, Phys. Rev. B **13**, 1633 (1976).

[19] T. G. Pedersen, H. Mera, and B. K. Nikolić, Phys. Rev. A **93**, 013409 (2016).

[20] E. Balslev and J. M. Combes, Commun. Math. Phys. **22**, 280 (1971).

[21] J. Aguilar and J. M. Combes, Commun. Math. Phys. **22**, 269 (1971).

[22] O. I. Tolstikhin, T. Morishita, and L. B. Madsen, Phys. Rev. A **84**, 053423 (2011).

[23] P. Cudazzo, C. Attaccalite, I. V. Tokatly, and A. Rubio, Phys. Rev. Lett. **104**, 226804 (2010).

[24] L. V. Keldysh, JETP Lett. **29**, 658 (1979).

[25] M. L. Trolle, T. G. Pedersen, and V. Véniard, Sci. Rep. **7**, 39844 (2017).

[26] M. Abramowitz, *Handbook of Mathematical Functions, With Formulas, Graphs, and Mathematical Tables* (Dover, New York, 1974).

[27] S. Koch, M. Kira, G. Khitrova, and H. M Gibbs, Nat. Mater. **5**, 523 (2006).

[28] M. Palummo, M. Bernardi, and J. C. Grossman, Nano Lett. **15**, 2794 (2015).

[29] H. Wang, C. Zhang, W. Chan, C. Manolatou, S. Tiwari, and F. Rana, Phys. Rev. B **93**, 045407 (2016).

[30] C. Poellmann, P. Steinleitner, U. Leierseder, P. Nagler, G. Plechinger, M. Porer, R. Bratschitsch, C. Schüller, T. Korn, and R. Huber, Nat. Mater. **14**, 889 (2015).

[31] H. Shi, R. Yan, S. Bertolazzi, J. Brivio, B. Gao, A. Kis, D. Jena, H. G. Xing, and L. Huang, ACS Nano **7**, 1072 (2013).

[32] D. Sun, Y. Rao, G. A. Reider, G. Chen, Y. You, L. Brézin, A. R. Harutyunyan, and T. F. Heinz, Nano Lett. **14**, 5625 (2014).

[33] A. J. F. Siegert, Phys. Rev. **56**, 750 (1939).

[34] C. W. McCurdy, M. Baertschy, and T. N. Rescigno, J. Phys. B **37**, R137 (2004).

[35] B. Simon, Phys. Lett. **71**, 211 (1979).

[36] C. W. McCurdy, C. K. Stroud, and M. K. Wisinski, Phys. Rev. A **43**, 5980 (1991).

[37] T. N. Rescigno and C. W. McCurdy, Phys. Rev. A **62**, 032706 (2000).

[38] T. Olsen, S. Latini, F. Rasmussen, and K. S. Thygesen, Phys. Rev. Lett. **116**, 056401 (2016).

[39] V. H. Trinh, O. I. Tolstikhin, L. B. Madsen, and T. Morishita, Phys. Rev. A **87**, 043426 (2013).

[40] P. A. Batishchev, O. I. Tolstikhin, and T. Morishita, Phys. Rev. A **82**, 023416 (2010).

[41] L. B. Madsen, O. I. Tolstikhin, and T. Morishita, Phys. Rev. A **85**, 053404 (2012).

[42] L. B. Madsen, F. Jensen, O. I. Tolstikhin, and T. Morishita, Phys. Rev. A **87**, 013406 (2013).

[43] X. L. Yang, S. H. Guo, F. T. Chan, K. W. Wong, and W. Y. Ching, Phys. Rev. A **43**, 1186 (1991).

[44] A. I. Dnestryan and O. I. Tolstikhin, Phys. Rev. A **93**, 033412 (2016).

[45] L. B. Madsen, F. Jensen, A. I. Dnestryan, and O. I. Tolstikhin, Phys. Rev. A **96**, 013423 (2017).

[46] A. I. Dnestryan, O. I. Tolstikhin, L. B. Madsen, and F. Jensen, J. Chem. Phys. **149**, 164107 (2018).

[47] H. Mera, T. G. Pedersen, and B. K. Nikolić, Phys. Rev. Lett. **115**, 143001 (2015).

[48] T. G. Pedersen, Phys. Rev. B **94**, 125424 (2016).

[49] L. S. R. Cavalcante, D. R. da Costa, G. A. Farias, D. R. Reichman, and A. Chaves, Phys. Rev. B **98**, 245309 (2018).

[50] A. Dalgarno, J. T. Lewis, and D. R. Bates, Proc. R. Soc. London, Ser. A **233**, 70 (1955).

[51] A. Scrinzi, Phys. Rev. A **81**, 053845 (2010); Eqs. (A1) and (A2) in that paper contain misprints. $(C^{-1})_{12}$ in Eq. (A1) should be replaced by $(C^{-1})_{21}$, and $(C^{-1})_{21}$ in Eq. (A2) should be replaced by $(C^{-1})_{12}$.

[52] V. I. Krylov, *Approximate Calculation of Integrals* (Dover, New York, 2005).

[53] A. Scrinzi and N. Elander, J. Chem. Phys. **98**, 3866 (1993).